INTERNATIONAL JOURNAL OF CLIMATOLOGY
Int. J. Climatol. (2015)
Published online in Wiley Online Library
(wileyonlinelibrary.com) DOI: 10.1002/joc.4568

RMetS
Royal Meteorological Society

Blind use of reanalysis data: apparent trends in Madden–Julian Oscillation activity driven by observational changes

Eric C. J. Oliver[a,b,c]*

[a] *Institute for Marine and Antarctic Studies, University of Tasmania, Hobart, Australia*
[b] *Australian Research Council Centre of Excellence for Climate System Science, Hobart, Australia*
[c] *Department of Oceanography, Dalhousie University, Halifax, Canada*

ABSTRACT: Atmospheric and oceanic reanalyses are used widely by the climate science community. These products provide full three-dimensional state fields and gapless time series, along with the confidence of being constrained by observational measurements, for atmospheric scientists and oceanographers to use in analyses of the climate system. However, as ubiquitous as reanalysis data are, it is not often considered how a scarcity of measurements in certain poorly observed regions, or over the course of a long period of time in which the observational system has changed significantly, impacts the realism of the data. This study explores this question using tropical surface pressures from the Twentieth Century Reanalysis to hindcast an index of the Madden–Julian Oscillation (MJO) over the 20th century. We show that by changing the choice of surface pressure predictor locations, and being aware of the observational measurements that have been assimilated by the reanalysis system, it is possible to control the estimated centennial-scale trend in MJO activity from nearly zero to an increase of 30% over the 20th century. We emphasize that this is an apparent trend as it arises solely from the use of reanalyzed surface pressures from locations that have either been poorly observed or have experienced significant changes in the observing system over the 20th century. This highlights the need to be aware of the observational measurements (or lack of them), particularly their density in space and time, that have been assimilated by a reanalysis system.

KEY WORDS reanalysis; Madden-Julian Oscillation; data assimilation; multidecadal variability; climate trends

Received 1 October 2014; Revised 13 September 2015; Accepted 22 October 2015

1. Introduction

For the last 20 years, meteorological and oceanographic reanalyses have provided climate researchers with data sets of great utility. A reanalysis provides a data set which synthesizes the merits of observations and numerical models. Namely, the quasi-observational nature of a reanalysis ensures that the data remain strongly constrained by observed variability, due to the assimilation of historical measurements, while the nature of the underlying unchanging numerical models ensures that the output contains no gaps or discontinuities in time or space as is common in the observational record. This provides a data set which can be used for a wide variety of studies of atmospheric, oceanographic, and climate variability. Frequently used reanalysis products include the National Centers for Environmental Prediction/National Center for Atmospheric Research (NCEP/NCAR) Reanalysis 1 (Kalnay *et al.*, 1996), the Japanese 25-year ReAnalysis [JRA-25, Onogi *et al.* (2007)], and the European Centre for Medium-Reange Weather Forecasts Interim Reanalysis [ERA-Interim, Dee *et al.* (2011)] for the atmosphere; the Simple Ocean Data Assimilation (SODA, Carton *et al.*, 2000a, 2000b), the French Global Ocean Reanalysis and Simulations [GLORYS, Bernard *et al.* (2006)], and Bluelink ReANalysis [BRAN, Oke *et al.* (2008); Schiller *et al.* (2008)] for the ocean; and the NCEP Climate Forecast System Reanalysis [CFSR, Saha *et al.* (2010)] for the coupled climate system.

There are two philosophical interpretations of what a reanalysis is. First, one can interpret a reanalysis as using observations to constrain a numerical model. This is the most common interpretation and relies on the data-assimilative nature of reanalyses whereby historical observational measurements of the atmosphere and ocean are 'assimilated' into a numerical model, using a variety of techniques [e.g. three-dimensional variational (3D-VAR), four-dimensional variational (4D-VAR); the Ensemble Kalman Filter; e.g. Evensen (2007)], in order to constrain an otherwise free-running numerical model to track as closely as possible the observed state trajectory. Second, one can interpret a reanalysis as using a numerical model to interpolate between, and extrapolate beyond, all available observations. All forms of interpolation and extrapolation use an underlying mathematical model to provide predictions where observations are missing. Data

* Correspondence to: E. C. J. Oliver, Institute for Marine and Antarctic Studies, University of Tasmania, Private Bag 129, Hobart, Tasmania 7001, Australia. E-mail: eric.oliver@utas.edu.au

assimilation and numerical models can be thought of as advanced interpolation methods (using our mathematical understanding of atmosphere and ocean dynamics) in time, space, and between geophysical parameters. Without such schemes, one has to revert to more simple schemes, e.g. linear interpolation, which assumes bit-wise linear data structures.

Both interpretations of a reanalysis given above are correct and allow us to understand the strengths and limitations of these products. One very important limitation is that if a reanalysis system is lacking observations for a particular period of time, or region of space, it will still provide an estimation of the full three-dimensional state of the atmosphere and/or ocean. (This could rightly be considered a feature, but for the purposes of this study, it is considered a limitation.) However, according to the first interpretation, a lack of observations implies that the underlying model is no longer being constrained by them, and the output is simply that of a free-running numerical model. (Note that even freely running numerical models are subject to boundary forcing, or background fields to which the model state is relaxed, and these may strongly constrain certain aspects of the variability in a way that is not strictly free.) Similarly, according to the second interpretation, interpolation and extrapolation schemes cannot cope with a complete lack of observations, and the model will relax to a state that is consistent with observations in other locations and the model's physics, but one that is not necessarily the true state of the system.

Clearly, it is important to consider the limitations of a reanalysis system when the spatial and temporal density of observations is very low. Previous studies have shown that changes to the observing system (i.e. changes to the frequency and/or locations of observations) have led to a spurious positive trend in sea level pressure in the Southern Hemisphere in the NCEP/NCAR Reanalysis (Hines *et al.*, 2000; Marshall and Harangozo, 2000), trends in Antarctic geopotential height and air temperature in the NCEP/NCAR Reanalysis (Marshall, 2002), and a warming trend in the lower troposphere in the ERA-40 reanalysis (Bengtsson *et al.*, 2004). This study reconstructs the variability of the Madden–Julian Oscillation (MJO) over the 20th century using surface pressures from the Twentieth Century Reanalysis (20CR), as done by Oliver and Thompson (2012), and demonstrates the implications of ignoring density of observations assimilated by the system. In doing so, we propose a method of overcoming this limitation by taking into account the density of assimilated observations in time and space.

2. Data and methods

The MJO is the dominant mode of intraseasonal atmospheric variability in the tropics (Madden and Julian, 1971, 1972, 1994; Wheeler and Hendon, 2004; Zhang, 2005). It consists of a region of deep convection, typically originating over the Indian Ocean, which then propagates eastward roughly following the equator. Strongly associated with the MJO are variations in cloud cover, precipitation, zonal wind in the lower and upper troposphere, and surface pressure. The temporal variability of the MJO is broad-banded with most energy on intraseasonal time scales between periods of about 30–90 days. We use the Wheeler and Hendon (2004) index to characterize the MJO. This bivariate index is based on the first two principal components of a multivariate combination of tropical outgoing longwave radiation and zonal wind at 200 and 850 hPa. We use daily values of the index over the 1979–2008 period, obtained from the Australian Bureau of Meteorology website (http://cawcr.gov.au/staff/mwheeler/maproom/RMM/). We have low-pass filtered the MJO index with a cutoff period of 10 days. This filtered index is denoted by I^{WH} and hereafter referred to as 'the MJO index'. We also calculated (1) the MJO amplitude, defined as the square root of the sum of the squares of the two components of the index, which is a measure of the strength of MJO activity, and (2) the MJO phase, defined as the angle of the two components of the index in phase space, discretized into eight integer values (Wheeler and Hendon, 2004).

The 20CR (Compo *et al.*, 2011) provides three-dimensional fields of the estimated atmospheric state from 1871 to the present. The reanalysis system uses a 56-member ensemble Kalman smoother and only assimilates surface and sea level pressures, sea surface temperature, and sea ice distribution in order to maintain a more constant observational system over the entire analysis period. This avoids, for example, potential shocks induced by the introduction of satellite data during the late 20th century. Daily fields of the ensemble mean and ensemble spread of surface pressure (p and Δp, respectively) on a 2°-resolution grid were obtained from 20CR (V2c) over the 1905–2008 period. The ensemble spread is a measure of the degree to which ensemble members have diverged from each other and tends to be large in the absence of observational measurements and small when the presence of observations are able to constrain the reanalysis estimates. In truth, this is an oversimplification and ensemble spread is also a function of the hydrodynamic flow itself as well as representing errors from both imperfect observations and an imperfect numerical model. Seasonal, interannual, and high-frequency variability were removed from the surface pressure time series following Oliver and Thompson (2012).

The MJO is represented strongly in 20CR surface pressure over the 1979–2008 period (Figure 1). Negative pressure anomalies develop over the Indian Ocean in phases 1–2 and propagate eastward through the Indo-Pacific in phases 3–4 and then into the eastern Pacific by phases 5–6. During phases 5–6, positive pressure anomalies develop over the Indian Ocean and propagate eastward out of phase (by four MJO phases) with the negative pressure anomalies. There is also poleward propagation of sea level pressure anomalies (notably over Asia from phases 3–4 to phases 5–6) which is possibly an expression of the Boreal Summer Intraseasonal Oscillation [e.g. Kikuchi *et al.* (2012)]. The proportion of MJO variability

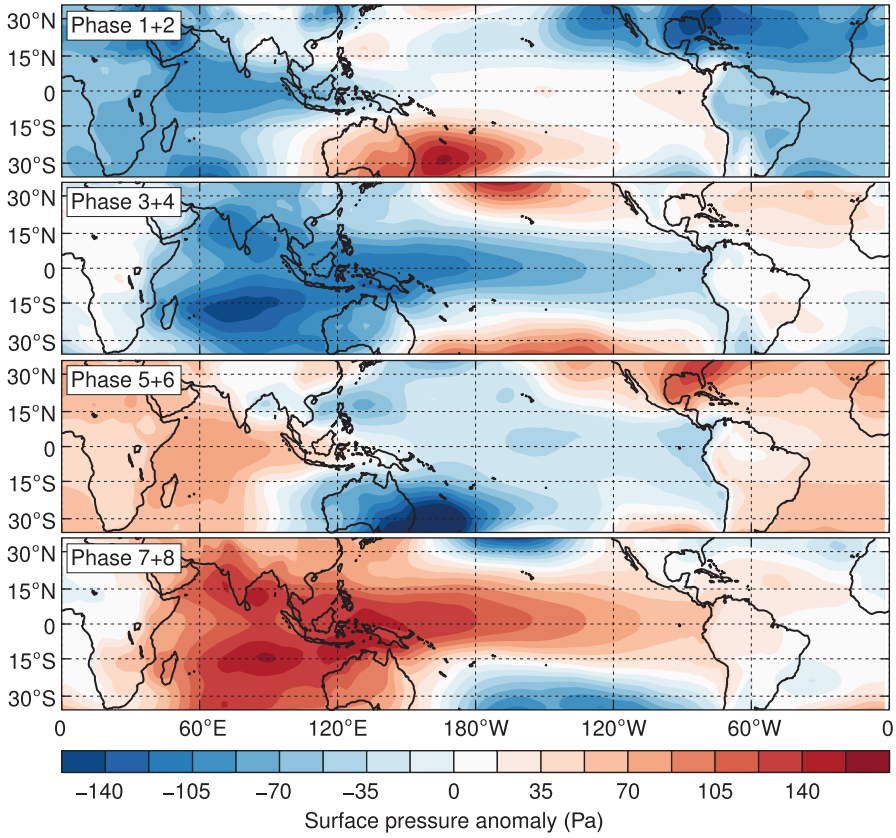

Figure 1. Relationship between the MJO and Twentieth Century Reanalysis surface pressures. Colours show composites of surface pressure anomalies over the 1979–2008 period with pairs of MJO phases (1 and 2 together, 3 and 4, etc.) based on the I^{WH} index.

that could be statistically accounted for by surface pressure was calculated at each location over the 1979–2008 period (Figure 2(a)). The metric used, $\overline{\kappa}$, was calculated at each location as the average coherence [e.g. Priestley (1981)] between I^{WH} and the surface pressure time series at that location, weighted according to the spectral density of I^{WH}. This metric is analogous to a correlation over intraseasonal time scales, i.e. a value of 1 indicates that 100% of the variability can be accounted for while a value of 0.5 indicates that only 50% of the variability can be accounted for (Oliver and Thompson, 2010, 2012). Time series of 20CR surface pressures clearly exhibit a strong statistical relationship with the MJO index throughout much of the tropics, particularly over the Indian and Pacific Oceans, explaining up to 65% of the variability in the Indo-Pacific warm pool. Therefore, we will use surface pressures from the 20CR as predictors of the state of the MJO.

We hindcasted an MJO index from time series of surface pressure at a finite number of locations using the multivariate linear regression model of Oliver and Thompson (2012). The model is of the form

$$\mathbf{I}_t = \beta \mathbf{p}_t + \varepsilon_t \qquad (1)$$

where $\mathbf{I}_t$ is the 2×1 bivariate MJO index at time t, β is a $2 \times m$ matrix of regression coefficients, $\mathbf{p}_t$ is a $m \times 1$ vector of surface pressure predictors (and their Hilbert transforms) at time t, and $\in_t$ is an error term. The time resolution was daily. Estimates of the regression coefficients $\widehat{\beta}$ were determined by an ordinary least squares fit of Equation (1) to the MJO index over the 1979–2008 period; the MJO index was then reconstructed over the 1905–2008 period using $\widehat{\mathbf{I}}_t = \widehat{\beta}\boldsymbol{p}_t$.

3. Results

We fit the model presented in Section 2 in three ways. First, in Section 3.1, we fit using surface pressures from locations chosen based on a simple model. In other words, we assumed that MJO-related variability of tropical surface pressure was well represented by 20CR and developed a simple model including locations which should contribute significant MJO-related variability. Second, in Section 3.2, we fit using surface pressures at locations chosen after taking into account the spatial and temporal density of the observations which were assimilated by 20CR. Finally, in Section 3.3, we purposefully choose a set of locations for which surface pressures are poorly observed.

3.1. Predictor locations chosen based on simple reasoning

The MJO is expressed strongly in surface pressure throughout much of the tropics [e.g. Madden and Julian (1972); also Figures 1 and 2(a)] and so, in the first instance, we sampled this region by choosing predictor locations distributed equally every 30° longitude along the equator

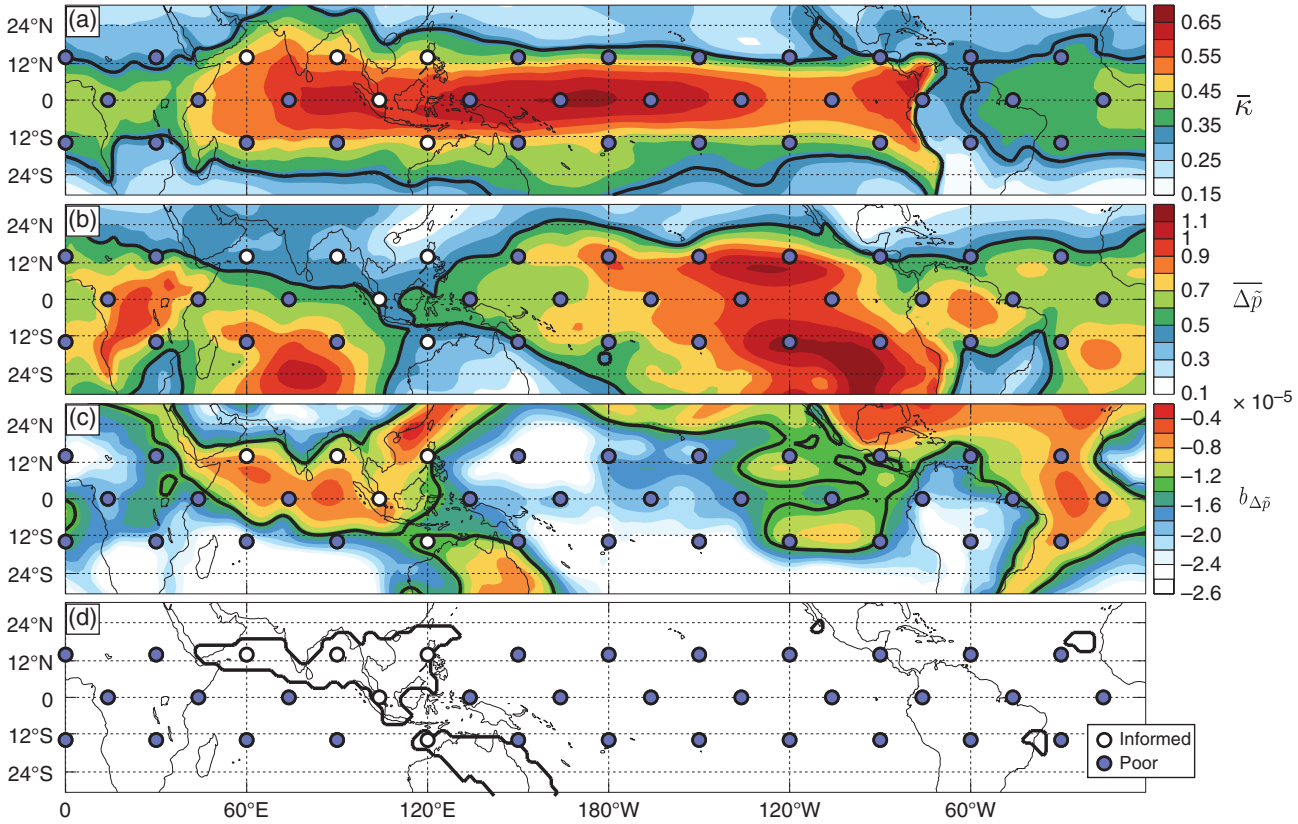

Figure 2. Observational feedback in model design. (a) The fraction of the total standard deviation of the MJO index that can be statistically accounted for by surface pressure. (b) and (c): measures of data uncertainty and stability, respectively, given by the time-mean $\overline{\Delta\tilde{p}}$ and linear trend $b_{\Delta\tilde{p}}$ of $\Delta\tilde{p}$. Thick contours indicate the critical values [(a) 0.33, (b) 0.5, and (c) -1.32×10^{-5} days^{-1}, respectively]. (d) The thick line delineates the combined area where $\overline{\kappa}$, $\overline{\Delta\tilde{p}}$, and $b_{\Delta\tilde{p}}$ are all below critical thresholds. Circles show the locations used for predictors in the Simple model; white circles show the subset of locations used in the Informed model, and the shaded blue circles show the subset used in the Poor model.

and along 14°N and 14°S, leading to a set of 36 locations from which to extract surface pressure time series $\mathbf{p}_t$ (Figure 2, all circles). This was called the 'Simple' model and later models consisted of a subset of points used in the Simple model.

The chosen pressure series $\mathbf{p}$ were fit to the MJO index over 1979–2008 and then hindcast over the 1905–2008 period using the model described in Section 2. The predicted MJO index, denoted I^{Sm}, captures I^{WH} well, with correlation coefficients of 0.89 and 0.87 for the first and second components, respectively (see Table 1). Time series of the components of I^{WH} and I^{Sm} over the 2000–2002 period demonstrate that I^{Sm} captures well the intraseasonal variability present in I^{WH} (Figures 3(a) and 4(a), black and blue lines). A cross-spectral analysis showed that I^{Sm} has a peak of energy in the same band of frequencies as I^{WH} and is highly coherent (>0.75) and in phase over those frequencies (Figure 5, black and blue lines). Note that the two components of the MJO index are more coherent with each other, outside of the intraseasonal band (30–90 days), for I^{Sm} than for I^{WH} indicating that the reconstructed index is capturing coherent non-intraseasonal variability not present in the original WH04 index. Time series of I^{Sm} over the 1920–1922 period also demonstrate that it exhibits similar intraseasonal variability (in character), although with a slightly lower amplitude, over the early 20th century (Figures 3(b) and 4(b), blue lines). This is confirmed by the similarity in power spectra calculated over the 1979–2008 period (Figure 5, solid blue line) and over the 1905–1978 period (Figure 5, dashed blue line). Also note that I^{Sm} and I^{WH} spend roughly the same proportion of time in each MJO phase (Table 2).

Table 1. Performance of predicted MJO indices for different choices of predictor locations.

Choice		ρ_1	ρ_2	Trend (century^{-1})
Simple	I^{Sm}	0.89	0.87	0.285 ± 0.023
Informed	I^{In}	0.69	0.70	0.0436 ± 0.025
Poor	I^{Po}	0.87	0.85	0.289 ± 0.023

Correlation coefficients between the Wheeler and Hendon (2004) index and predicted MJO indices are shown for the first and second components (ρ_1 and ρ_2, respectively) along with the linear trend over the 20th century (±95% confidence interval) in MJO amplitude of the predicted index for each of the model fits.

Time series of the MJO amplitude (smoothed with a 10-year moving average) of I^{WH} and I^{Sm} indicate similar linear trends (-0.102 century^{-1} and -0.164 century^{-1}, respectively) and a number of shared interannual variations over the shared 1979–2008 period (Figure 6, black and blue lines). However, over the entire record (1905–2008), the MJO amplitude of I^{Sm} exhibits a strong positive trend

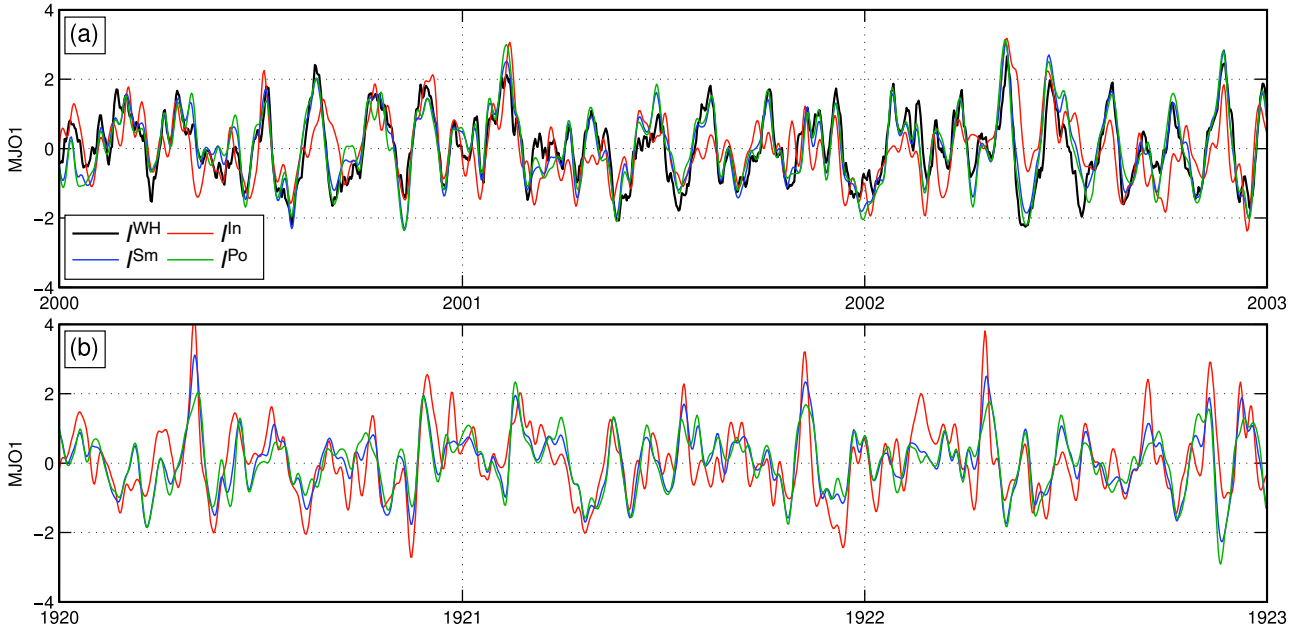

Figure 3. Time series of the Wheeler and Hendon (2004) and predicted MJO indices (first component). The first component of I^{WH} (black), I^{Sm} (blue), I^{In} (red), and I^{Po} (green) are shown plotted over (a) 2000–2002 and (b) 1920–1923 (except I^{WH}).

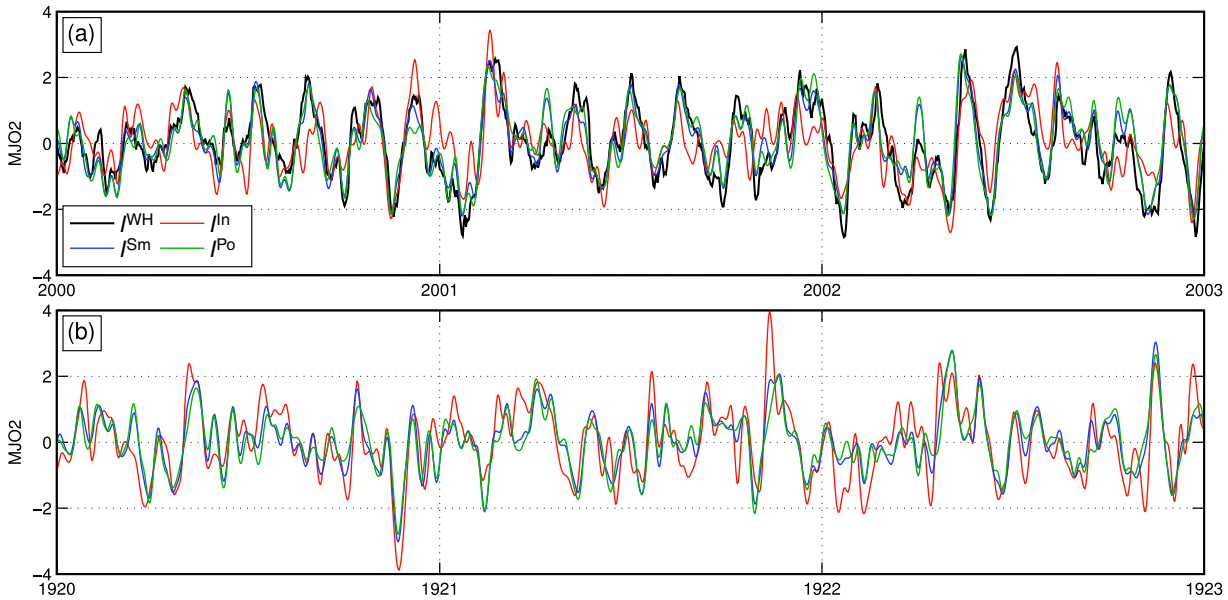

Figure 4. Time series of the Wheeler and Hendon (2004) and predicted MJO indices (second component). The first component of I^{WH} (black), I^{Sm} (blue), I^{In} (red), and I^{Po} (green) are shown plotted over (a) 2000–2002 and (b) 1920–1923 (except I^{WH}).

with time. The magnitude of this trend is 0.285 ± 0.023 century^{-1} (see also Table 1). This corresponds to an increase in MJO amplitude of ∼30% over the 20th century. Is this trend realistic or a consequence of our choice of predictors from a potentially imperfect reanalysed variable? We address this question in the following subsection.

3.2. Predictor locations chosen based on observational feedback

We now wish to choose predictors by taking into account the density of observational measurements in time and space that have informed the 20CR reanalysis. Information on the observations that have been assimilated by 20CR, what we call here observational feedback, is readily available (Compo *et al.*, 2011). The surface pressures assimilated by 20CR are detailed and available in their original form as part of the International Surface Pressure Databank (ISPD). The ISPD is made up of three parts: station observations, marine (ship-based) observations, and tropical cyclone observations. The station component is largely drawn from the International Surface Database [ISD; Lott *et al.* (2008)], the marine component from the International Comprehensive Ocean Atmosphere Data Set [ICOADS; Worley *et al.* (2005)], and the tropical cyclone

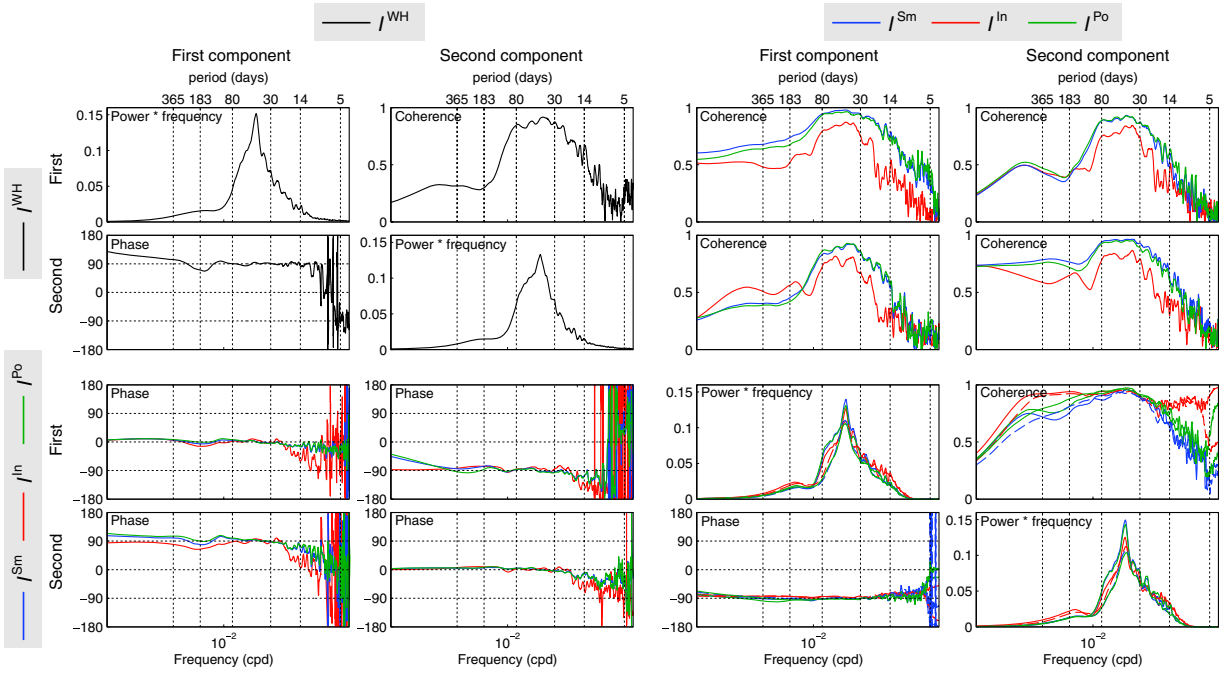

Figure 5. Cross-spectral analysis of I^{WH} and the predicted MJO indices. The power spectral densities are shown in the diagonal panels and the coherence and phase spectra in the above-diagonal and below-diagonal panels, respectively. Solid lines indicate that the spectra were calculated from data over the 1979–2008 period and dashed lines indicate that they were calculated from data over the 1905–1978 period.

Table 2. Proportion of days (in %) spent in each phase for I^{WH} and for the predicted index for each of the model fits.

Index	Phase 1	Phase 2	Phase 3	Phase 4	Phase 5	Phase 6	Phase 7	Phase 8
I^{WH}	13.3	13.5	11.8	12.2	12.9	12.4	12.2	11.7
I^{Sm}	12.8	12.3	12.5	12.3	13.2	12.3	11.9	13.0
I^{In}	13.8	13.2	12.2	11.1	12.6	12.8	11.6	12.6
I^{Po}	12.1	12.0	12.7	12.8	12.8	12.2	12.1	13.3

component from the International Best Track Archive for Climate Stewardship [IBTrACS; Knapp *et al.* (2010)]. Summary data for these databases are publicly available, e.g. location and time period for active stations in ISPD. Furthermore, 20CR provides fields of ensemble spread which can also be related to observational data density.

Considering the time span covered by 20CR, there is unsurprisingly considerable variation in the density of observational measurements over time. For example, there were clearly many more surface pressure observations available from both station- and ship-based platforms, both of which were assimilated by 20CR, in the late 20th century as compared to the early 20th century (Figure 7). The total number of stations recording in the tropics (equatorward of $\pm 30^{\circ}$ latitude) over four subsets of the 20th century was 80 (1900–1925), 1156 (1926–1950), 22 762 (1951–1975), and 28 024 (1976–2000); the average number of ship observations per month over the same area was 1.29×10^4 (1900–1925), 2.26×10^4 (1926–1950), 6.42×10^4 (1951–1975), and 7.31×10^4 (1976–2000).

The ensemble spread of surface pressure from 20CR, Δp, can be used as a measure of how the density of observational measurements varies in time and space (G. Compo, 2009; pers. comm.). In the limiting case of no observations, the ensemble members of the reanalysis system will each act as a freely running model and so diverge within the natural variability expected of the chaotic climate system, leading to a large value of Δp. In the case of many observations, the ensemble members will converge due to the presence of observations constraining their evolution and limiting the degree to which they can diverge, leading to a small value of Δp. Regions of high (low) observational density will have low (high) values of Δp. Because the magnitude of surface pressure variations depends on spatial location, we normalize Δp at each location by the standard deviation of reanalysis surface pressure at that location through time σ leading to the normalized ensemble spread (NES) of surface pressure $\Delta\widetilde{p}$:

$$\Delta\widetilde{p} = \frac{\Delta p}{\sigma}. \tag{2}$$

We will refer to large (small) values of $\Delta\widetilde{p}$ as high (low) uncertainty reanalysis data.

We wish to estimate an MJO index that is both (1) accurate (e.g. correlated with I^{WH}), and (2) stable (in its level of uncertainty) over the entire estimation period. This will require predictors that have both (1) low data uncertainty, and (2) little or no trend in data uncertainty over the record

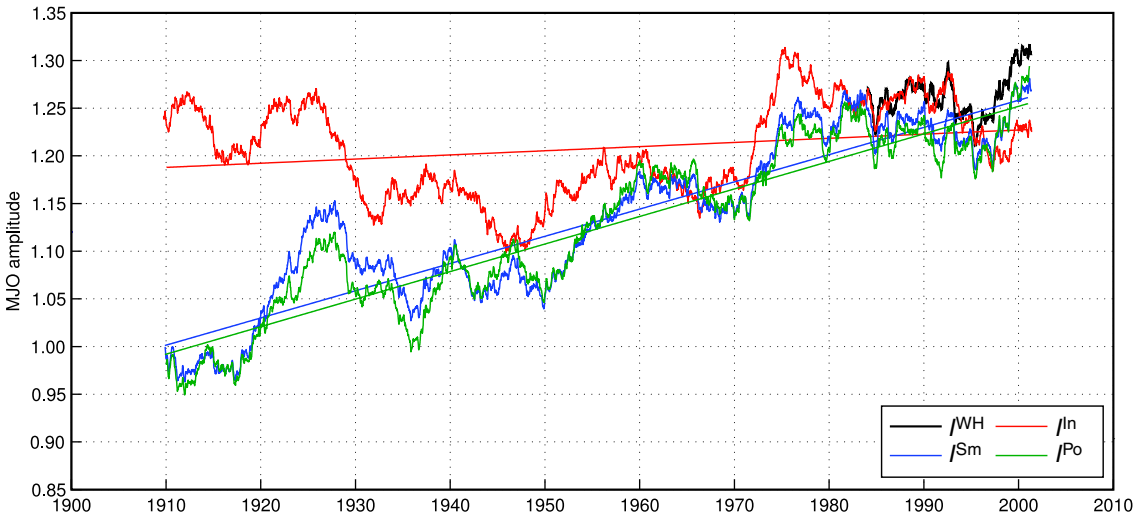

Figure 6. Time series of MJO amplitude of the Wheeler and Hendon (2004) and predicted MJO indices. The MJO amplitude, after smoothing with a moving 10-year average, is shown over the 20th century for I^{WH} (black), I^{Sm} (blue), I^{In} (red), and I^{Po} (green). Corresponding straight lines indicate the linear trend of each predicted index over the 1905–2008 period.

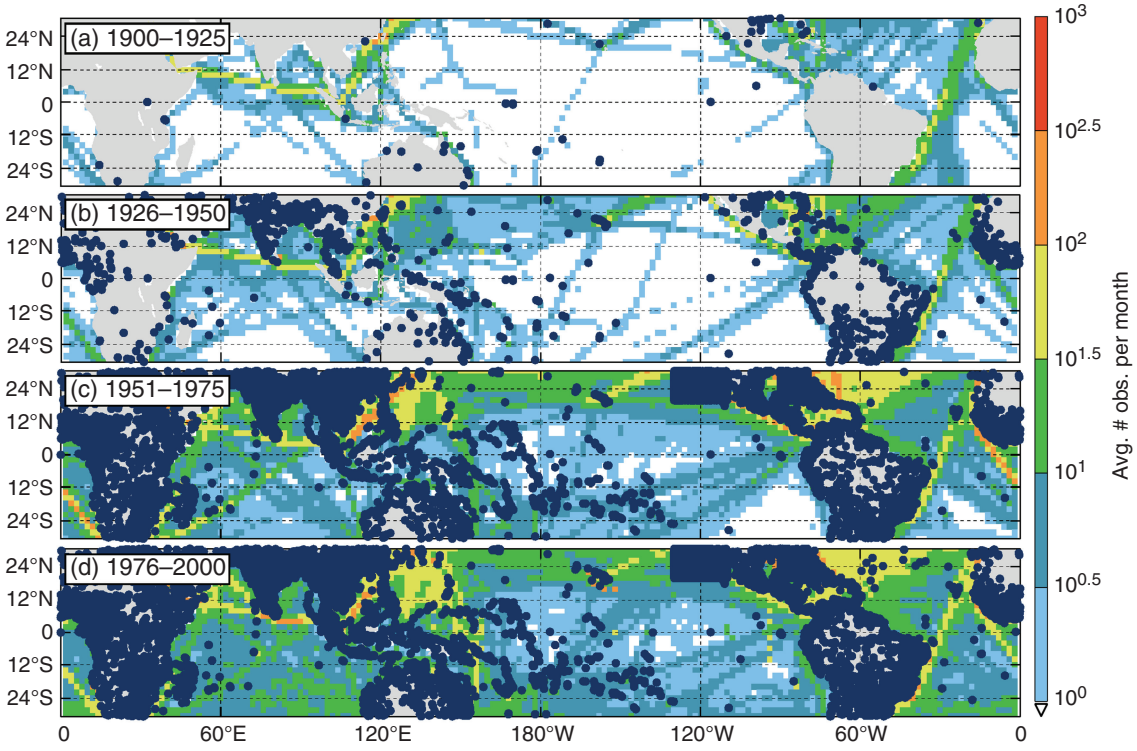

Figure 7. Maps demonstrating the changes to the surface pressure observing system over the 20th century. Colours indicate average number of ship observations per month (on a logarithmic scale; locations with less than 1 observation per month are masked white) and dark blue dots indicate the presence of station measurements during the following time periods: (a) 1900–1925, (b) 1926–1950, (c) 1951–1975, and (d) 1976–2000.

length. We calculated the mean ($\overline{\Delta\widetilde{p}}$) and linear trend ($b_{\Delta\widetilde{p}}$) of $\Delta\widetilde{p}$ over the 1905–2008 period (Figure 2(b) and (c)). As expected $\overline{\Delta\widetilde{p}}$ is generally low in regions with a high density of observations over the 20th century (e.g. the North Indian Ocean, off Southeast Asia, Australia, the southeast coast of Brazil, North America; compare Figures 2(b) and 7). The linear trend $b_{\Delta\widetilde{p}}$, which has been defined so that positive indicates an increase of $\Delta\widetilde{p}$ with time, reflects local changes in the observing system and tends to be low where the number of measurements has been largely consistent over time (e.g. the Eastern Pacific, the Tropical Atlantic and Indian, eastern Australia; compare Figures 2(b) and 7). Note that $b_{\Delta\widetilde{p}}$ is always negative, i.e. there are no locations in space where $\Delta\widetilde{p}$ increases with time. We have ensured low data uncertainty and stability by excluding from consideration locations where $\overline{\Delta\widetilde{p}} > 0.5$ and $b_{\Delta\widetilde{p}} < -1.32 \times 10^{-5}$ days^{-1} [thick contours, Figure 2(b) and (c)]. These values correspond to an ensemble spread

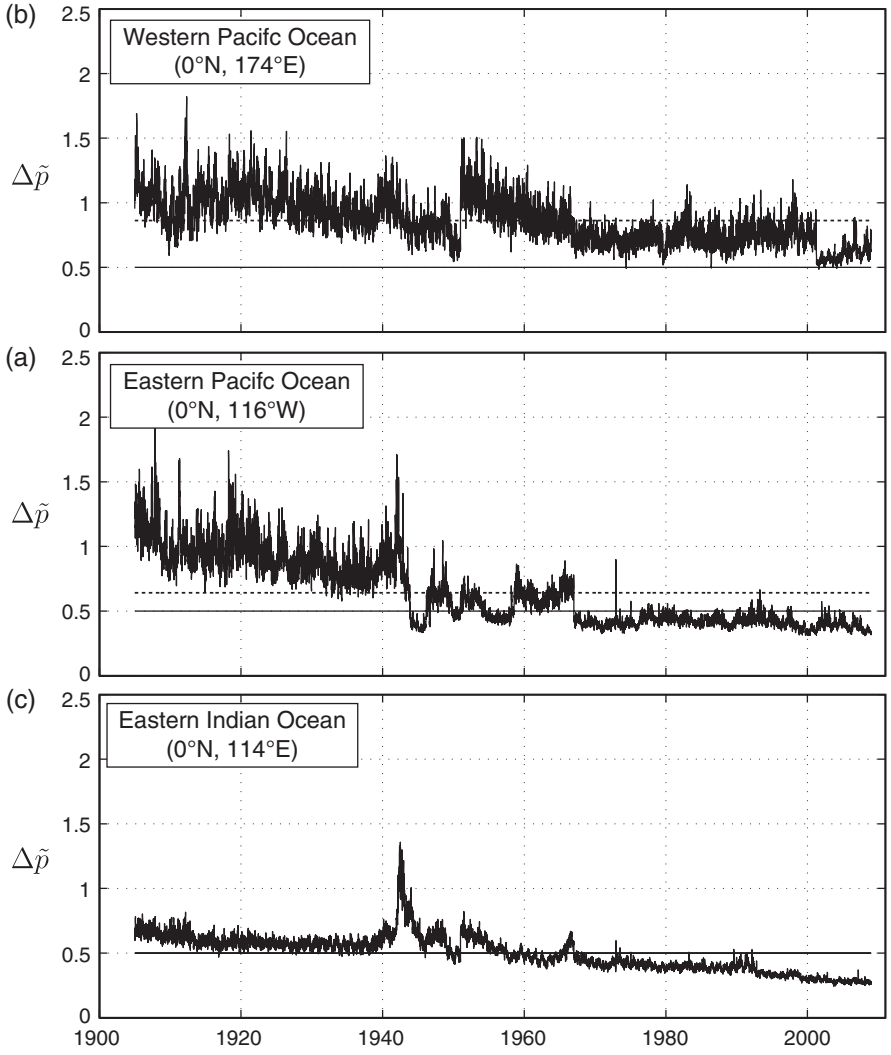

Figure 8. Data uncertainty and stability at three example locations. Time series of the normalized ensemble spread $\Delta\widetilde{p}$ are shown over the 20th century at locations in (a) the Eastern Pacific Ocean, (b) the Western Pacific Ocean, and (c) the Eastern Indian Ocean (solid lines). The value of $\overline{\Delta\widetilde{p}}$ for each time series is shown by a dashed horizontal line and the critical threshold ($\overline{\Delta\widetilde{p}} = 0.5$) is shown as a solid line. Note that the value of $\overline{\Delta\widetilde{p}}$ in panel (c) is only marginally below the critical threshold, so the two horizontal lines are indistinguishable.

that is half the surface pressure variability ($\Delta\widetilde{p} < 0.5$ on average) and a change in $\Delta\widetilde{p}$ that is 1/2 over the entire record. Note that this choice was arbitrary and only made to ensure a relatively low data uncertainty (low mean value of $\Delta\widetilde{p}$) and stability (weak trend in $\Delta\widetilde{p}$); other choices could function just as well, but these were used to illustrate sensitivity to observational data density.

Example time series of $\Delta\widetilde{p}$ for selected locations in the Eastern and Western Pacific Oceans and in the Eastern Indian Ocean are shown in Figure 8. These locations were chosen as good examples to illustrate cases which did not meet the thresholds outlined above (the Pacific Ocean examples) and a case which did (the Indian Ocean example). In the Eastern Pacific Ocean, there have never been many land- or ship-based observations, so the value of $\Delta\widetilde{p}$ has remained high over the entire record leading to a region of high data uncertainty from which to derive predictors (Figure 8(a)). Predictors from this region were rejected based on the condition requiring $\overline{\Delta\widetilde{p}} \leq 0.5$. In the Western Pacific Ocean, there was a dramatic change in the observing system: from nearly no observations prior to 1940 to a very well observed region afterwards (Figure 8(b)). This was reflected in the dramatic change in $\Delta\widetilde{p}$ pre- and post-1940 leading to an unstable region from which to derive predictors; predictors from this region were rejected based on the condition requiring $b_{\Delta\widetilde{p}} \geq -1.32 \times 10^{-5}$. The Eastern Indian Ocean has been well observed over the course of the 20th century with very few major changes to the observing system. Predictors from this region were accepted as of low uncertainty ($\overline{\Delta\widetilde{p}} \leq 0.5$) and stable over the entire record [$b_{\Delta\widetilde{p}} \geq -1.32 \times 10^{-5}$ days^{-1}; Figure 8(c)].

Predictor locations were chosen by taking into account both reasoning based on statistical relationships and data uncertainty and stability. Simple reasoning takes into account the statistical connection between the MJO index and surface pressure using the $\overline{\kappa}$ metric limiting the domain from which predictor locations can be selected to regions

Table 3. Linear trend over the 20th century in MJO amplitude, within each MJO phase, of the predicted index for each of the model fits.

Index	Phase 1	Phase 2	Phase 3	Phase 4	Phase 5	Phase 6	Phase 7	Phase 8
I^{Sm}	0.257	0.209	0.262	0.456	0.262	0.303	0.279	0.281
I^{In}	0.0154	-5.70×10^{-3}	8.45×10^{-5}	0.0574	0.0509	0.129	0.0814	0.035
I^{Po}	0.272	0.182	0.288	0.475	0.242	0.274	0.280	0.320

Units are century^{-1}.

where $\overline{\kappa} \geq 0.33$ [Figure 2(a), thick contour]. As above, this choice was arbitrary and only made to ensure surface pressures statistically account for a fair proportion of MJO variability; other choices are just as valid but this was chosen for illustrative purposes. We have also taken into account data uncertainty and stability using the above criteria for $\overline{\Delta\widetilde{p}}$ and $b_{\Delta\widetilde{p}}$, and the thick contour in Figure 2(d) shows the combined exclusion region based on the combined criteria. This led to a set of five locations from which to extract surface pressure time series p [Figure 2(d), white circles].

The chosen pressure series $\mathbf{p}$ were fit to the MJO index over 1979–2008 and then hindcast over the 1905–2008 period as in Section 3.1. Again, the predicted MJO index, denoted I^{In} (the 'Informed' fit), captured well the variability of I^{WH}, with correlation coefficients of 0.69 and 0.70 the two components (see Table 1) which is supported by plots of the time series (Figures 3 and 4, red line). It should be noted that the lower correlation coefficients, as compared with the Simple fit, are reflected in the time series with a number of departures of I^{In} from I^{WH}, particularly at oscillation periods shorter than MJO variability. In fact, a cross-spectral analysis showed that while I^{In} did have a peak of energy in the same band of frequencies as I^{WH}, it was slightly less coherent over this band than was I^{Sm} (0.50–0.85) and much less so at higher frequencies (e.g. coherence was <0.5 for periods less than 20 days; Figure 5, black and red lines). Also note that I^{In} and I^{WH} spend roughly the same proportion of time in each MJO phase (Table 2). Similarly, the MJO amplitude of I^{In} is similar to the amplitude of I^{WH} (Figure 6, red line). However, it is notable that the amplitude of I^{In} has a much weaker trend than I^{Sm} over the 1905–2008 record: 0.0436 ± 0.025 century^{-1}. This trend is barely significantly different from zero with 95% confidence.

3.3. Predictor locations chosen with large data uncertainty and stability

A further fit was performed where predictor locations were purposely chosen from regions with large data uncertainty and stability. These predictors, denoted the 'Poor' fit, were the subset of predictors used for the Simple fit which did not satisfy the selection criteria outline above [Figure 2(d), blue dots]. Again, the predicted MJO index, denoted I^{Po}, captured I^{WH} well, with correlation coefficients of 0.87 and 0.85 for the two components (see Table 1) which is supported by plots of the time series (Figures 3 and 4, green line), high coherence with I^{WH} (Figure 5, green lines), and a similar proportion of time spent in each MJO phase (Table 2). However, the trend in MJO amplitude of I^{Po} (Figure 6, green line) is now notably much larger than I^{In} and similar to the trend in I^{Sm}: 0.289 ± 0.023 century^{-1} (an increase of ~30% over the 20th century).

The region from which predictor locations were chosen for the Informed fit was most strongly affected by active MJO convection in phases 2 through 5, while the regions sampled for the Poor fit are affected in other phases [e.g. Wheeler and Hendon (2004)]; the Simple fit on the other hand used predictor locations which sampled more evenly the tropics. Did phases corresponding to active convection in regions with large data uncertainty and stability exhibit the same long-term trends in all three indices, or was the observational feedback (used to develop the Informed fit) able to provide improved information across MJO phases despite a regionalization of predictor locations? We calculated the trend in MJO amplitude within each MJO phase to determine if this regional restriction of predictor locations impacts MJO activity unevenly across MJO phases (Table 3). While there is phase-dependency in the trend for each fit there remains a large difference in trend between I^{In} and both I^{Sm} and I^{Po}, just as for the all-phase trend. Also note that all indices spend roughly the same proportion of time in each MJO phase as I^{WH} (Table 2). Therefore, the Informed fit is not restricted to only providing improved information for phases which active MJO convection lies within the region sampled by predictor locations.

4. Summary and discussion

In this study, we have examined the impact of spatial and temporal variations in the density of observational measurements assimilated by a reanalysis system on estimates of long-term climate variability. Specifically, we fit 20CR surface pressures to the Wheeler and Hendon (2004) MJO index over the 1979–2008 period and, provided with a satisfactory fit, hindcast the MJO index back to 1905. We showed that three different choices of predictor locations in the tropics each provided an acceptable fit to MJO variability characterized by the Wheeler and Hendon (2004) index, generally capturing the timing and relative amplitude of major events. However, these choices provided dramatically different long-term trends in estimated MJO activity. In the case of predictor locations informed only by the statistical relationship between the MJO and tropical surface pressure, we estimated a trend in MJO activity of 0.285 ± 0.023 century^{-1} over the 20th century. We then

used observational feedback to take into account the temporal and spatial density of observational measurements assimilated by the reanalysis system and restricted our choice of predictors accordingly which lead to an estimated trend in MJO activity of nearly zero (0.0436 ± 0.025 century^{-1}). We further demonstrated that by purposefully choosing predictors from locations where the density of observational measurements assimilated by a reanalysis system was low and/or changed significantly over time lead, we could find a strong estimated trend in MJO activity (0.289 ± 0.023 century^{-1}). By changing the location (and therefore the uncertainty of the reanalysis data) from which predictors are chosen, we have been able to maintain a good fit to the Wheeler and Hendon (2004) index over the 1979–2008 period while modifying the trend over the 20th century of the estimated index by nearly a factor of ten.

The results of this article highlight one of the potential pitfalls of using reanalysis data blindly without considering the underlying data. It is important when using reanalysis data to have an understanding of the nature of the observations that have (or have not) been assimilated by it and the deficiencies of the underlying numerical model. This is particularly the case for climate phenomena which are often poorly simulated in free-running models, such as the MJO. In such cases with a lack of observations, a reanalysis system reverts to the predictions from a free-running model, i.e., without an accurate representation of the climate phenomenon of interest. On the other hand, in the presence of observations, the reanalysis system is constrained to represent the climate phenomenon in a more realistic manner. Therefore, this study reinforces that care needs to be taken when using reanalysis data, and it should not be assumed that they are a substitute for observations or are a perfect representation of the climate system.

It should be noted that the specific results of this study, namely the representation of the MJO in 20CR through surface pressures, should not be generalized to other reanalysis products. For example, it is quite possible that the expressions of the MJO in surface pressures from the NCEP/NCAR Reanalysis or ERA-Interim are very accurate. The reason for the specific findings of this study is due to the heterogeneous spatial and temporal density of tropical surface pressure observations assimilated by 20CR. This does not imply that reanalyses are generally poor at reconstructing the MJO but only that an understanding of the observational density is important when using any reanalysis.

Acknowledgements

The author acknowledges Prof Keith Thompson (Department of Oceanography, Dalhousie University) for helpful discussions and Dr Phil Klotzbach (Department of Atmospheric Science, Colorado State University) for comments. The author also thanks the anonymous reviewers for their helpful and insightful comments.

References

Bengtsson L, Hagemann S, Hodges KI. 2004. Can climate trends be calculated from reanalysis data? *J. Geophys. Res.* **1090**(D1111): 1–8.

Bernard B, Madec G, Penduff T, Molines J-M, Treguier A-M, Le Sommer J, Beckmann A, Biastoch A, Böning C, Dengg J, Derval C, Durand E, Gulev S, Remy E, Talandier C, Theetten S, Maltrud M, McClean J, De Cuevas B. 2006. Impact of partial steps and momentum advection schemes in a global ocean circulation model at eddy-permitting resolution. *Ocean Dyn.* **560**(5–6): 543–567.

Carton JA, Chepurin G, Cao X. 2000a. A simple ocean data assimilation analysis of the global upper ocean 1950-95. Part II: results. *J. Phys. Oceanogr.* **300**(2): 311–326.

Carton JA, Chepurin G, Cao X, Giese B. 2000b. A simple ocean data assimilation analysis of the global upper ocean 1950-95. Part I: methodology. *J. Phys. Oceanogr.* **300**(2): 294–309.

Compo GP, Whitaker JS, Sardeshmukh PD, Matsui N, Allan RJ, Yin X, Gleason BE, Vose RS, Rutledge G, Bessemoulin P, Bronnimann S, Brunet M, Crouthamel RI, Grant AN, Groisman PY, Jones PD, Kruk MC, Kruger AC, Marshall GJ, Maugeri M, Mok HY, Nordli Ø, Ross TF, Trigo RM, Wang XL, Woodruff SD, Worley SJ. 2011. The twentieth century reanalysis project. *Q. J. R. Meteorol. Soc.* **1370**(654): 1–28.

Dee DP, Uppala SM, Simmons AJ, Berrisford P, Poli P, Kobayashi S, Andrae U, Balmaseda MA, Balsamo G, Bauer P, Bechtold P, Beljaars ACM, van de Berg L, Bidlot J, Bormann N, Delsol C, Dragani R, Fuentes M, Geer AJ, Haimberger L, Healy SB, Hersbach H, Holm EV, Isaksen L, Kallberg P, Kohler M, Matricardi M, McNally AP, Monge-Sanz BM, Morcrette J-J, Park B-K, Peubey C, de Rosnay P, Tavolato C, Thepaut J-N, Vitart F. 2011. The ERA-Interim reanalysis: configuration and performance of the data assimilation system. *Q. J. R. Meteorol. Soc.* **1370**(656): 553–597.

Evensen G. 2007. *Data Assimilation*. Springer: Berlin, Germany.

Hines KM, Bromwich DH, Marshall GJ. 2000. Artificial surface pressure trends in the NCEP-NCAR reanalysis over the southern ocean and Antarctica. *J. Clim.* **130**(22): 3940–3952.

Kalnay E, Kanamitsu M, Kistler R, Collins W, Deaven D, Gandin L, Iredell M, Saha S, White G, Woollen J, Zhu Y, Leetmaa A, Reynolds R, Chelliah M, Ebisuzaki W, Higgins W, Janowiak J, Mo KC, Ropelewski C, Wang J, Jenne R, Joseph D. 1996. The NCEP/NCAR 40-year reanalysis project. *Bull. Am. Meteorol. Soc.* **770**(3): 437–471.

Kikuchi K, Wang B, Kajikawa Y. 2012. Bimodal representation of the tropical intraseasonal oscillation. *Clim. Dyn.* **38**: 1989–2000.

Knapp KR, Kruk MC, Levinson DH, Diamond HJ, Neumann CJ. 2010. The international best track archive for climate stewardship (IBTrACS) unifying tropical cyclone data. *Bull. Am. Meteorol. Soc.* **910**(3): 363–376.

Lott N, Vose R, Del Greco SA, Ross TF, Worley S, Comeaux J. 2008. The integrated surface database: partnerships and progress. In *Preprints*, *24th Conference on Interactive Information Processing Systems*, New Orleans, LA, American Meteorological Society B, Volume 3.

Madden RA, Julian PR. 1971. Detection of a 40–50 day oscillation in the zonal wind in the Tropical Pacific. *J. Atmos. Sci.* **280**(5): 702–708.

Madden RA, Julian PR. 1972. Description of global-scale circulation cells in the tropics with a 40–50 day period. *J. Atmos. Sci.* **290**(6): 1109–1123.

Madden RA, Julian PR. 1994. Observations of the 40–50-day tropical oscillation – a review. *Mon. Weather Rev.* **1220**(5): 814–837.

Marshall GJ. 2002. Trends in Antarctic geopotential height and temperature: a comparison between radiosonde and NCEP-NCAR reanalysis data. *J. Clim.* **150**(6): 659–674.

Marshall GJ, Harangozo SA. 2000. An appraisal of NCEP/NCAR reanalysis MSLP data viability for climate studies in the South Pacific. *Geophys. Res. Lett.* **270**(19): 3057–3060.

Oke PR, Brassington GB, Griffin DA, Schiller A. 2008. The Bluelink ocean data assimilation system (BODAS). *Ocean Model.* **210**(1–2): 46–70.

Oliver ECJ, Thompson KR. 2010. Madden-Julian Oscillation and sea level: local and remote forcing. *J. Geophys. Res.* **1150**(C1): C01003.

Oliver ECJ, Thompson KR. 2012. A reconstruction of Madden-Julian Oscillation variability from 1905 to 2008. *J. Clim.* **250**(6): 1996–2019.

Onogi K, Tsutsui J, Koide H, Sakamoto M, Kobayashi S, Hatsushika H, Matsumoto T, Yamazaki N, Kamahori H, Takahashi K, Kadokura S, Wada K, Kato K, Oyama K, Ose T, Mannoji N, Taira R. 2007. The jra-25 reanalysis. *J. Meteorol. Soc. Jpn. Ser. II* **850**(3): 369–432.

Priestley MB. 1981. *Spectral Analysis and Time Series*. Academic Press: New York, NY.

Saha S, Moorthi S, Pan HL, Wu X, Wang J, Nadiga S, Tripp P, Kistler R, Woollen J, Behringer D, Liu H, Stokes D, Grumbine R, Gayno G, Wang J, Hou Y-T, Chuang H-Y, Juang H-M H, Sela J, Iredell M, Treadon R, Kleist D, Van Delst P, Keyser D, Derber J, Ek M, Meng J, Wei H, Yang R, Lord S, Van Den Dool H, Kumar A, Wang W, Long C, Chelliah M, Xue Y, Huang B, Schemm J-K, Ebisuzaki W, Lin R, Xie P, Chen M, Zhou S, Higgins W, Zou C-Z, Liu Q, Chen Y, Han Y, Cucurull L, Reynolds RW, Rutledge G, Goldberg M. 2010. The NCEP climate forecast system reanalysis. *Bull. Am. Meteorol. Soc.* **910**(8): 1015–1057.

Schiller A, Oke PR, Brassington G, Entel M, Fiedler R, Griffin DA, Mansbridge JV. 2008. Eddy-resolving ocean circulation in the Asian–Australian region inferred from an ocean reanalysis effort. *Prog. Oceanogr.* **760**(3): 334–365.

Wheeler MC, Hendon HH. 2004. An all-season real-time multivariate MJO index: development of an index for monitoring and prediction. *Mon. Weather Rev.* **1320**(8): 1917–1932.

Worley SJ, Woodruff SD, Reynolds RW, Lubker SJ, Lott N. 2005. ICOADS release 2.1 data and products. *Int. J. Climatol.* **250**(7): 823–842.

Zhang C. 2005. Madden-Julian Oscillation. *Rev. Geophys.* **43**: 1–36.

